Photodetachment of the outer shell of C^- in the excited ^2D state

H.-L. Zhou* and S. T. Manson†
Department of Physics and Astronomy, Georgia State University, Atlanta, Georgia 30303, USA

A. Hibbert
Department of Applied Mathematics and Theoretical Physics, Queen's University, Belfast BT7 1NN, United Kingdom

L. Vo Ky and N. Feautrier
DAMAP, UMR 8588 du CNRS, Observatoire de Paris, 92195 Meudon Cedex, France
(Received 26 May 2005; published 21 September 2005)

Photodetachment of the outer shells of the excited ^2D state of C^- using an augmented R-matrix theoretical methodology has been studied from threshold to 11 eV. Total and partial cross sections and photoelectron angular distribution asymmetry parameters have been obtained. Excellent agreement between length and velocity formulations is found. In addition, agreement with experiment at 2.076 eV for both cross section and β for photodetachment to the ground $2s^22p^2\ ^3P$ state of C is quite good. The results exhibit many examples of Auger decay of shape resonances. Comparison with a previous calculation shows fair agreement except near threshold.

DOI: 10.1103/PhysRevA.72.032723 PACS number(s): 32.80.Gc, 32.80.Fb

I. INTRODUCTION

Negative atomic ions are present in a variety of situations. Their structure and dynamics are determined largely by many-body electron-electron interactions, i.e., correlation [1–4]. Thus, studies of negative ion photoabsorption (photodetachment) provide stringent tests of how well the theory deals with electron-electron correlation. In addition, since the coupling of the incident photon with the target ion is weak, information about both initial bound and final continuum states is obtained from photodetachment studies.

The photodetachment of open-shell negative ions is of particular interest owing to the existence of significant $l \rightarrow l+1$ transitions to the unfilled outer subshell. Such transitions were seen to be extremely important in both inner- and outer-shell photodetachment of He^- [5–9]. In fact the $1s \rightarrow 2p$ transition that produced the $2s2p^2$ autoionizing state was so strong in He^- that it could be detected from the production of He^+ resulting from a very weak double Auger process [9].

In a previous paper, a study of the photodetachment of another open-shell negative ion was reported; the ground ^4S state of C^- [10]. This investigation, using an augmented R-matrix theoretical methodology, resolved the discrepancies then extant among previous calculations [11–14]. Of particular interest is that the C^- ion is one of the very few negative atomic ions possessed of a bound excited state. In this paper, the photodetachment of this exited state, which is an excited ^2D multiplet of the same $1s^22s^22p^3$ configuration as the ground ^4S state, is considered. We focus particularly upon an understanding of the photodetachment cross section, along with how the different initial state coupling (and binding energy) causes the excited ^2D state photodetachment cross section to differ from the photodetachment cross section of the ground ^4S state multiplet.

The photodetachment of the ^2D state of C^- was considered in a previous R-matrix calculation [11] and comparison is made with the results. In addition, there is a measurement of the cross section [15] and the photoelectron angular distribution [16] at a single photon energy 2.079 eV; comparison is made with the measurements as well.

In the next section, the theoretical approach is discussed. The following section presents and discusses our results. And the final section gives a summary and conclusions.

II. THEORETICAL DETAILS

An approach based on R-matrix theory [17,18] has been employed in the present photodetachment calculations. The methodology employed in the present paper is the same as used in the previous work on photodetachement of C^- in the ^4S ground state [10]. The photodetachment of the excited state of the negative C^- ion considered herein is given by

$$C^-(1s^22s^22p^3)^2D + h\nu \rightarrow [C + e]^2S,P,D. \qquad (1)$$

The methodology employed can be broken up into the calculation of the N-electron states of the final-state atom, the neutral carbon atom (often called the target states, for historical reasons), and the calculation of the $(N+1)$-electron wave functions of the $C+e$ final states and the C^- initial state.

A. States of neutral carbon

At low energies, only outer-shell photodetachment is energetically possible. The detachment of $2s$ or $2p$ from the $1s^22s^22p^3\ ^2D$ state of C^- leads to either $1s^22s^22p^2$ or $1s^22s2p^3$ states of C. However, detachment *plus* excitation can also occur, so that the possible states of the neutral carbon include $1s^22s^22pnl$ and $1s^22s2p^2nl$; the K shell remains essentially inert. Since the initial state of the C^- ion is ^2D, we

*Corresponding author. Electronic address: zhou@phy-astr.gsu.edu
†Electronic address: smanson@gsu.edu

need to include singlet and triplet neutral carbon atomic states.

We represent the wave functions Φ_i for these atomic states by means of configuration-interaction (CI) expansions in terms of configuration state functions (CSFs) ψ_j:

$$\Phi_i(L_iS_i) = \sum_{j=1}^{M} a_{ij}\psi_j(\alpha_j L_i S_i) \tag{2}$$

with the angular momenta coupled according to α_j to form a total L_iS_i. The coefficients a_{ij} are the eigenvector components of the Hamiltonian matrix whose typical element is $\langle\psi_j|H_N|\psi_k\rangle$, where H_N is the N-electron Hamiltonian. The corresponding eigenvalues E_i of any $L_iS_i\pi$ symmetry are the calculated target-state energies of neutral C, and satisfy the inequalities

$$E_i \geqslant E_i^{\text{exact}}. \tag{3}$$

The M basis functions ψ_j are constructed from one-electron orbitals of the form

$$\frac{1}{r}P_{nl}(r)Y_l^{m_l}(\theta,\phi)\chi_{m_s}(\sigma). \tag{4}$$

The radial functions $P_{nl}(r)$ in these calculations are expressed in analytic form as

$$P_{nl}(r) = \sum_{j=1}^{k} C_{jnl}N_{jnl}r^{I_{jnl}}\exp(-\zeta_{jnl}r) \tag{5}$$

where N_{jnl} is the normalization factor

$$N_{jnl} = \left(\frac{(2\zeta_{jnl})^{2I_{jnl}+1}}{(2I_{jnl})!}\right)^{1/2}. \tag{6}$$

Except for $1s,2s,2p$, the value of k has been set equal to $n-l$, so that the coefficients C_{jnl} are uniquely determined by the orthonormality requirements

$$\int_0^\infty P_{nl}(r)P_{n'l}(r)dr = \delta_{nn'}. \tag{7}$$

The CI calculation is performed using the CIV3 code [19].

The states of C that have been included in the calculation are $[1s^2]2s^22p^2$, $2s2p^3$, $2s^22p3s$, $2s^22p3p$, $2s^22p3d$, $2s2p^23s$, $2s2p^23p$, $2p^33s$, and $2p^33p$. We shall refer to these configurations as the reference set. To begin with, it is necessary to generate radial functions for each of the orbitals occupied in the dominant configuration(s) of the above states. The radial $1s,2s,2p$ orbitals are the Hartree-Fock HF functions of $1s^22s^22p^2\ ^3P$ given by [20], the $3s$ and $3p$ orbitals are obtained by optimizing the energies of the $2s^22p3s\ ^3P^o$ and $2s^22p3p\ ^3D$ states of carbon, respectively. The $3d$ orbital is optimized on the polarizability of the carbon ground state $2s^22p^2\ ^3P$; in our previous work on Li [21–23], it was found that including states that model the polarizability of the ground state of the target atom was important. Hence the state labeled $2s^22p3d$ will correspond to a polarized pseudostate rather than to a spectroscopic state. Correlation effects are introduced using the orbitals $4s$, $4p$, and $4d$, optimized on the energy of $2s^22p^2\ ^3P$. With this set of orbitals, we constructed CSFs by allowing all one- and two-electron replacements of orbitals in configurations of the reference set.

The bound energy of the initial ^2D state of C^- is only about 30 meV. This is much smaller than that of the ^4S ground state of C^-, which is about 1.26 eV. We found that, in this calculation of ^2D photodetachment in C^-, when we excluded the $4f$ orbital, we were unable to obtain a bound initial state, but that this problem was overcome by including the configurations $2s^22p4f$ and $2p^34f$, with the $4f$ orbital optimized on the $2s^22p^2\ ^1D$ state. We have added these configurations for the present calculation. This resulted in a total of 3806 CSFs covering all the $LS\pi$ symmetries of the carbon states. The optimized radial function parameters are displayed in Table I.

Note that the $3d$, $4s$, $4p$, $4d$, and $4f$ orbitals are *not* spectroscopic. Thus, although a large CI expansion, Eq. (2), is used for each physical state Φ_i, those states where the predominant configuration contains nonspectroscopic orbitals are likely to be somewhat less accurate representations of the carbon atom wave functions. Thus, only the physical states for which the dominant term is composed of spectroscopic orbitals are considered accurate enough to serve as final channels in the cross-section caculations. These are listed in Table II.

Also in Table II, comparison with experimental energies from the NIST website [32] is made. Given that we have used only three correlation orbitals, plus $4f$ in a limited way, the agreement between the calculated and experimental energy differences is reasonably good. Therefore we are confident that our wave functions provide a sufficiently good representation of the states of neutral carbon for use in the R-matrix calculations.

B. Initial and final states of the (C+e) system

The wave functions for the initial $1s^22s^22p^3\ ^2D$ excited state of C^- and final continuum states $^2P,^2D,$ $^2F(N+1)$-electron systems are calculated using the same one-electron orbitals as for the N-electron states of neutral carbon, with the addition of 30 continuum basis orbitals for each orbital angular momentum of the continuum electron of $l\leqslant 4$, since discrete orbitals up to $n=4$, $l=3$ are included. The R-matrix radius was chosen as $a=23.4a_0$ in order to enclose almost completely the discrete orbitals. Since we consider low energy, only outer-shell photodetachment is possible; the inner-shell $1s$ orbital cannot be excited. The $(N+1)$-electron wave functions for the initial state of C^- and the final continuum state of the $C+e$ system are then constructed from the N-electron functions in the standard R-matrix manner [18,21], using discrete orbitals up to $4f$ and continuum orbitals as described above. In the present calculation, we include all 48 neutral carbon states in the close-coupling expansion. In addition, for completeness, purely discrete $(N+1)$-electron terms are added. These are generated from the N-electron ψ_j (introduced above) by the addition of one more electron in all possible configurations, using orbitals up to $4f$. But in order to get the best bounded initial state and convergent final continuum state, we add different terms for the initial ^2D state and final states.

TABLE I. Orbital parameters.

nl	C_{jnl}	I_{jnl}	ζ_{jnl}	nl	C_{jnl}	I_{jnl}	ζ_{jnl}
1s	0.89523	1	5.53875	3p	0.29197	2	1.87789
	0.07720	1	9.25013		−0.99821	3	0.50335
	0.00413	2	2.04126				
	0.03954	2	5.30567	3d	1.00000	3	0.93824
	−0.00123	2	1.30552				
				4s	0.71844	1	3.00743
2s	−0.18039	1	5.53875		−2.37858	2	2.12304
	−0.02141	1	9.25013		2.13007	3	1.75046
	0.57726	2	2.04126		−0.54103	4	0.74042
	−0.08643	2	5.30567				
	0.50920	2	1.30552	4p	2.49278	2	1.46703
					−2.78945	3	1.52292
2p	0.56470	2	1.44037		0.48677	4	0.59045
	0.22955	2	2.60786				
	0.26761	2	0.96499	4d	1.15948	3	1.98827
	0.01016	2	6.53286		−0.72151	4	1.13329
3s	0.09751	1	4.73923	4f	1.00000	4	2.12182
	−0.37056	2	1.82295				
	1.03213	3	0.64121				

Using the same formalism, but with bound-state (closed-channel) boundary conditions, the initial-state wave function of the negative C^- ion is generated. The excited C^- is very weakly bound. The calculated electron affinity of the $1s^2 2s^2 2p^2\ ^3P$ state of carbon is 0.004 Ry(54 meV), in reasonable agreement with the experimental value of 33 meV [24]. This agreement gives some indication of the quality of our initial-state wave function; in the present calculation, all energies are *ab initio*; no energy shifts are introduced anywhere.

III. RESULTS AND DISCUSSION

A. Partial cross sections

Unlike the situation for photodetachment of the ground ^4S state of C^-, where only ^4P final states are possible, the photodetachment of the excited ^2D states leads to ^2P, ^2D, and ^2F final states of the $C+e^-$ system. In this calculation, the cross sections leading to the lowest 13 triplet and singlet states of neutral carbon have been considered, as listed in the previous

TABLE II. Comparison of energies (eV) of the final-state channels of neutral C employed in the calculation, relative to the ground state of neutral C. Also listed are the possible partial waves for each of the final states of C. The underlined partial waves indicate that a single-particle transition from the initial ^2D state of C^- is possible.

Final atomic state[a]	Energy	Experiment	^2P	^2D	^2F
$C(2s^2 2p^2\ ^3P)$	0.0000	0.0000	$\underline{\epsilon s}, \underline{\epsilon d}$	$\underline{\epsilon d}$	$\underline{\epsilon d}, \epsilon g$
$C(2s^2 2p^2\ ^1D)$	1.3298	1.2601	$\underline{\epsilon d}$	$\underline{\epsilon s}, \underline{\epsilon d}, \epsilon g$	$\underline{\epsilon d}, \epsilon g$
$C(2s^2 2p^2\ ^1S)$	2.9117	2.6803		ϵd	
$C(2s^2 2p 3s\ ^3P^o)$	7.3847	7.4816	ϵp	$\epsilon p, \epsilon f$	ϵf
$C(2s^2 2p 3s\ ^1P^o)$	7.6129	7.6811	ϵp	$\epsilon p, \epsilon f$	ϵf
$C(2s 2p^3\ ^3D^o)$	8.0248	7.9423	$\underline{\epsilon p}, \epsilon f$	$\underline{\epsilon p}, \epsilon f$	$\underline{\epsilon p}, \epsilon f$
$C(2s 2p^2 3s\ ^1P)$	8.4325		$\epsilon s, \epsilon d$	ϵd	$\epsilon d, \epsilon g$
$C(2s^2 2p 3p\ ^3D)$	8.5454	8.6408	ϵd	$\epsilon s, \epsilon d, \epsilon g$	$\epsilon d, \epsilon g$
$C(2s^2 2p 3p\ ^3S)$	8.6790	8.7675		ϵd	
$C(2s^2 2p 3p\ ^3P)$	8.7853	8.8457	$\epsilon s, \epsilon d$	ϵd	$\epsilon d, \epsilon g$
$C(2s^2 2p 3p\ ^1D)$	9.0247	8.9989	ϵd	$\epsilon s, \epsilon d, \epsilon g$	$\epsilon d, \epsilon g$
$C(2s^2 2p 3p\ ^1S)$	9.3614	9.1682		ϵd	
$C(2s 2p^3\ ^3P^o)$	9.5716	9.3268	ϵp	$\epsilon p, \epsilon f$	ϵf

[a] $1s^2$ is omitted for simplicity.

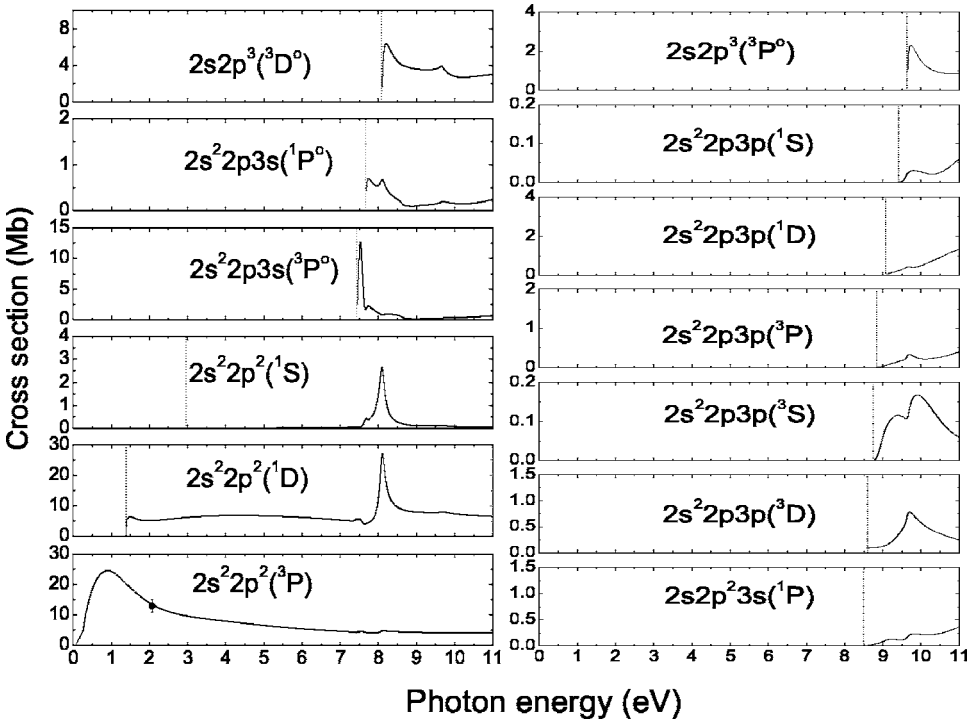

FIG. 1. Photodetachment cross sections of the excited ^2D state of C^- for producing the various states of neutral carbon as a function of photon energy calculated in length gauge. Also shown is the experimental point [15] at 2.076 eV for producing C in the ground state. The vertical dotted lines represent the various thresholds.

section; since we are dealing with an initial state that is a doublet, quintet states of C are forbidden.

The calculated total photodetachment cross sections for producing each of the 13 states of C, i.e., the sums over the ^2P, ^2D, and ^2F partial cross sections, are given in Fig. 1. The calculated partial cross sections for photodetachment leading to each of these 13 final states of neutral carbon are shown in Fig. 2 for the ^2P manifold, Fig. 3 for the ^2D manifold, and Fig. 4 for the ^2F manifold. Although the calculations have been performed in both length and velocity formulations, only length is shown in Figs. 1–4 to avoid confusion. The agreement between length and velocity, as will be demonstrated later, is quite good.

1. Below the $2s^22p^2\ ^1D$ threshold

Below the $2s^22p^2\ ^1D$ threshold, only the $2s^22p^2\ ^3P$ photodetachment channels are open. The photodetachment cross section for producing the $2s^22p^2\ ^3P$ of neutral carbon is

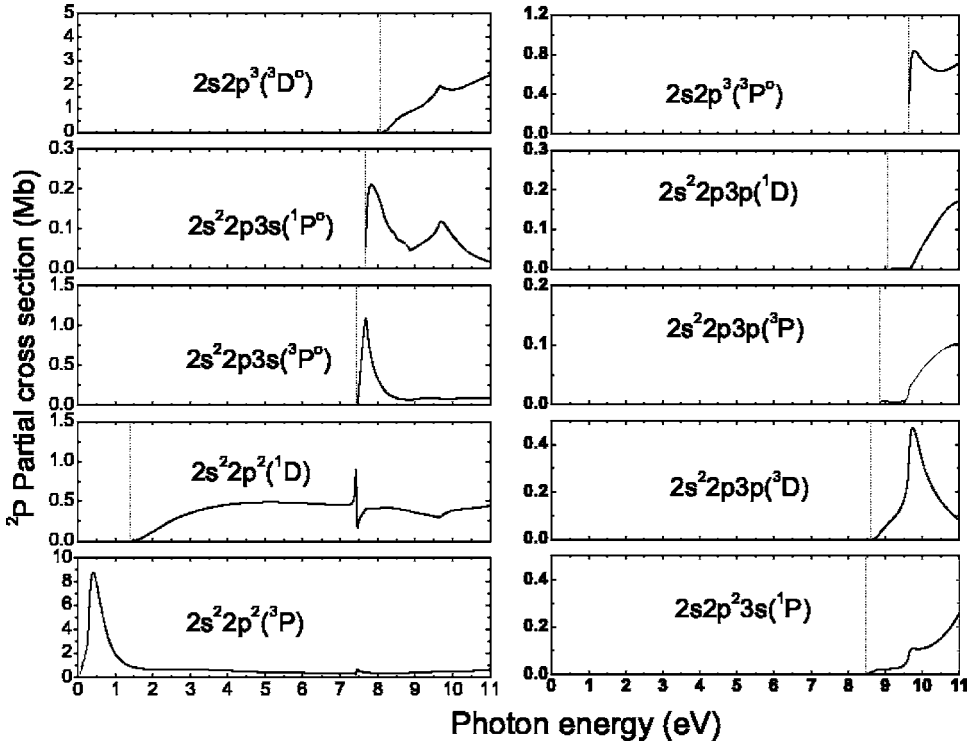

FIG. 2. Partial ^2P photodetachment cross sections of the excited ^2D state of C^- for producing the various states of neutral carbon as a function of photon energy calculated in length gauge. The vertical dotted lines represent the various thresholds.

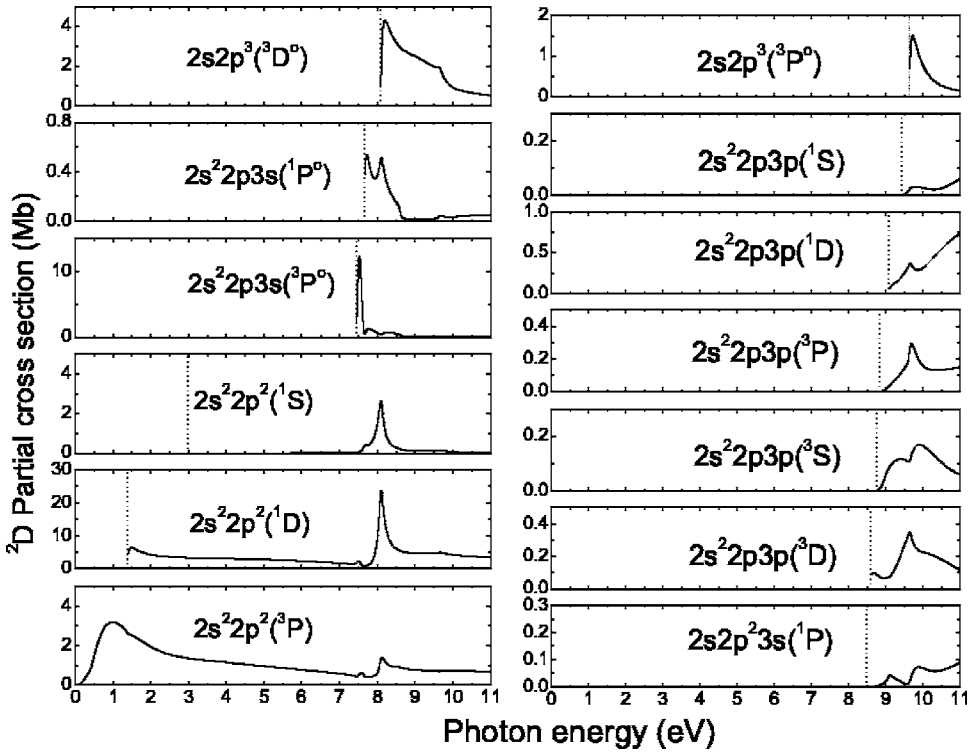

FIG. 3. Partial ^2D photodetachment cross sections of the excited ^2D state of C^- for producing the various states of neutral carbon as a function of photon energy calculated in length gauge. The vertical dotted lines represent the various thresholds.

given in Fig. 1 where it is seen that the cross section, starting from a zero threshold value (an intrinsic feature of photodetachment), reaches a value of almost 25 Mb about 1 eV above threshold, before tailing off at higher energies. This is essentially a single-electron process, as listed in Table II, $2p \rightarrow \epsilon s$, which appears only in the ^2P manifold owing to angular momentum considerations, and $2p \rightarrow \epsilon d$, which appears in ^2P, ^2D, and ^2F manifolds; the partial cross sections to each of these manifolds are shown in Figs. 2–4. The ^2D and ^2F partial cross sections each show a maximum at about 1 eV above threshold that arise from $2p^2(^3P)3d$ shape resonances. The ^2F maximum is seen to be about a factor of 6 larger than the ^2D; this is due primarily to the angular factors in the cross section (the relative multiplet strengths [25]) which are 126 and 22.5 for the ^2F and ^2D transitions, respectively, very close to a factor of 6. For the ^2P partial cross section the maximum of about 9 Mb is located at approximately 0.3 eV; this is due to the $2p^2(^3P)3s$ shape resonance.

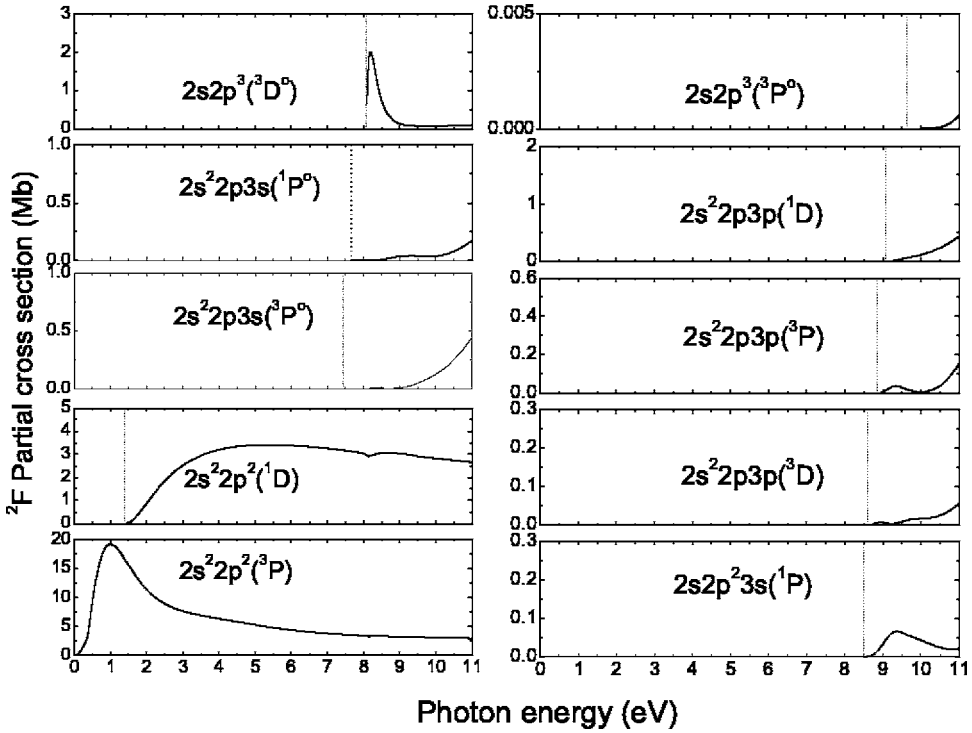

FIG. 4. Partial ^2F photodetachment cross sections of the excited ^2D state of C^- for producing the various states of neutral carbon as a function of photon energy calculated in length gauge. The vertical dotted lines represent the various thresholds.

It is at lower energy because a $p \rightarrow s$ photodetachment cross section increases from threshold as $\epsilon^{0.5}$ while a $p \rightarrow d$ transition increases much more slowly as $\epsilon^{1.5}$. In addition, there is no hint of the *d*-wave resonance that should appear in the ^2P partial cross section as well. It actually is there, but the relative multiplet strength is so small, only 1.5, that the cross section of a few tenths of a megabarn is not discernible above the background of the $p \rightarrow s$ transition. The details of the individual resonances in each of the partial cross section are obliterated in the total cross section for $2s^2 2p^2\ ^3P$ production, as seen in Fig. 1.

2. Between the $2s^2 2p^2\ ^1D$ and $2s^2 2p^2\ ^1S$ thresholds

In the region between the second and third detachment thresholds, photodetachment to the first excited state of neutral carbon, $2s^2 2p^2\ ^1D$, is now possible. The cross section for this transition is seen in Fig. 1 where a 6 Mb threshold maximum, followed by a shallow dip and a broad second maximum, appears. This cross section too is made up of single-electron transitions, as seen in Table II, with the exception of the ϵg possibility that occurs in the ^2D and ^2F partial cross sections. The threshold maximum is a $2p^2(^1D)3s$ shape resonance in the ^2D partial cross section, as seen in Fig. 3. Since this resonance lies *above* the $2s^2 2p^2\ ^1D$ threshold, it can autodetach to the continuum via a $3s \rightarrow \epsilon s$ transition which is the predominant mode of decay. However, this resonance can also autodetach to the ground $2s^2 2p^2\ ^3P$ state, and this is seen in Fig. 3 as a small window resonance in the $2s^2 2p^2\ ^3P$ partial cross section. In addition, all three partial cross sections are seen to exhibit a $p \rightarrow d$ maximum, a gradual rise from threshold that is partially obliterated by the *s*-wave shape resonance in the ^2D partial cross section. Unlike the $p \rightarrow d$ transitions leading to the ground state of carbon, however, in this channel these transitions do not have a significant shape resonance component.

As mentioned above, there is also an ϵg component in the ^2D and ^2F partial cross sections. Our results find these to be rather negligible, however, with cross sections several orders of magnitude below the *s*- and *d*-wave cross sections.

In this energy region, there is a measurement of the cross section for producing the ground $2s^2 2p^2\ ^3P$ state of neutral carbon at a single photon energy effected using photoelectron spectroscopy [15], and this result is shown in Fig. 1. Agreement with the present theoretical result is seen to be excellent, which provides some indication of the accuracy of the calculation. The experiment reported a value of 13 ± 2 Mb, and the present calculation finds 13.36 and 12.85 Mb in length and velocity formulations, respectively. The experimental result also compares favorably with a previously calculated value [15] of 13.8 Mb. However, it must be noted that comparison at a single energy, while indicative, is hardly conclusive.

3. Between the $2s^2 2p^2\ ^1S$ and $2s^2 2p3s\ ^3P$ thresholds

In this broad energy range, from about 2.96 to 7.44 eV, the $2s^2 2p^2\ ^1S$ photodetachment channel opens; only an ϵd photoelectron in the ^2D partial cross section contributes, as seen in Table II. The calculated results for this channel are shown in Figs. 1 and 3 and the cross sections are too small to be seen on the scale employed. The reason is that this cross section is forbidden at the single-particle level because the $2p^3\ ^2D$ initial state of C^- has no $2p^2\ ^1S$ parent. This cross section can only gain strength though interchannel coupling, which is insignificant in this energy range, or through Auger decay, which is energetically forbidden in this region. Of course, since the cross section to the $2s^2 2p^2\ ^1S$ state is so small, there are no interchannel effects on other cross sections.

4. Between the $2s^2 2p3s\ ^3P$ and $2s^2 2p3s\ ^1P$ thresholds

The newly opened channels in this energy region involve photodetaching transitions to the $2s^2 2p3s\ ^3P^o$ state of neutral carbon. This is the first case of the dominant transitions involving detachment plus electronic excitation. It is seen from Table II that an ϵp continuum wave contributes to the ^2P and ^2D partial cross section, while ϵf contributes to ^2D and ^2F. A strong $2p3s3p$ resonance in the ^2D partial cross section (Fig. 3), which "decays" to the $2p3s\ ^3P$ state of neutral carbon, dominates the cross section for producing the newly accessible state; as seen in Fig. 1 the cross section maximizes at about 13 Mb. This resonance can also autodetach to each of the $2p^2$ lower states of carbon, and the effect of this autodetachment on these cross sections is also seen in Fig. 3. In particular, the $2s^2 2p^2\ ^1S$ cross section rises from its essentially zero value due to this autodetachment. This is another example of the Auger decay of a shape resonance.

The existence of such a strong resonance in a detachment-plus-excitation channel is evidence for the extent to which correlation affects the photodetachment process, in this case a very significant (roughly 50%) $2p^2 3p$ correlation mixing in the $2p^3$ initial state; this mixing was found from a multiconfiguration Hartree-Fock calculation. The $2p3s3p$ resonance is reached by a strong (one-electron) $2p \rightarrow 3s$ transition from the $2p^2 3p$ correlation.

In addition, a rather less strong $2p3s3p$ resonance, about an order of magnitude smaller due to angular factors in the dipole matrix element, in the ^2P partial cross section, shown in Fig. 2, is seen, which also has significant autodetachment to the lower states; the $2s^2 2p^2\ ^1D$ partial cross section shows a classic Fano profile in the ^2P manifold. Note that the maxima of the ^2P and ^2D resonances are at slightly different positions due to dynamical effects.

The ^2F partial cross section contains only an *f* wave, and is, thus, quite small in this energy range, as seen in Fig. 4. Further, the *f*-wave contribution to the ^2D partial cross section is also quite small in this energy range.

5. Between the $2s^2 2p3s\ ^1P$ and $2s2p^3\ ^3D$ thresholds

In this energy region, the $2s^2 2p3s\ ^1P$ channels open. These are similar to the ones that opened in the previous energy region with the difference that these transitions are to the singlet state of neutral carbon, rather than the triplet state; the configurations, however, are the same. The calculated total cross section for producing the $2s^2 2p3s\ ^1P$ state is given in Fig. 1, where a threshold maximum is seen. As in the triplet case discussed above, this maximum arises from

the $2p3s3d$ resonance at the thresholds of the ^2P and ^2D partial cross sections, as seen in Figs. 2 and 3 respectively, but unlike the triplet case, the ^2P and ^2D resonances have similar strengths. That this feature is really a shape resonance, and not simply a threshold maximum is evident in that the Auger decay to lower channels is seen in Fig. 1.

Both the ^2P and particularly the ^2D partial cross sections are much weaker than their counterparts in the triplet cross sections. Since they are weak, the Auger transitions to lower channels are also weaker, but still observed. The relative weakness of the ^2D partial cross section leading to the singlet final state of neutral carbon is due partly to the angular factor which favors the triplet partial cross section by a factor of 3, along with the fact that in the ^3P state of carbon, the $3s$ wave function is more compact compared to the ^1P owing to the attractive exchange interaction in the ^3P state as compared to a repulsive interaction in the ^1P state. Similar considerations apply to the ^2P partial cross section.

The ^2F partial cross section has no resonance and is quite small in this energy region, just as it was for the triplet case, and for the same reasons.

6. Between the $2s2p^3\ ^3D$ and the $2s2p^2 3s\ ^1P$ thresholds

In this region the lowest inner-shell photodetachment cross section, the $2s2p^3\ ^3D$ cross section, becomes energetically possible. As indicated in Table II, there is a single-particle $2s \rightarrow \epsilon p$ transition in each partial cross section, ^2P, ^2D, and ^2F. There is also an ϵf wave contributing to each partial cross section, but in each case, the ϵf contribution is several orders of magnitude smaller than the ϵp. This is primarily because the transitions to the $(2s2p^3\ ^3D)\ \epsilon p$ final states are *single-particle* transitions, while correlation is required to get to the $(2s2p^3\ ^3D)\ \epsilon f$ final states.

The calculated photodetachment cross section leading to the $2s2p^3\ ^3D$ state of neutral carbon is shown in Fig. 1 where a large (about 6 Mb) threshold maximum is seen. The origin of this maximum can be understood by looking at the partial cross sections. The ^2D partial cross section, Fig. 3, shows a large shape resonance just above threshold, which is found to be mostly $2s2p^4$, but is fairly strongly mixed with other configurations, notably $2s2p^3 3p$; this mixing is characteristic of negative ions for which single-configuration designations are far less adequate than for neutral atoms. In any case, this resonance is populated by a strong $2s \rightarrow 2p$ single-particle transition. This is seen to Auger decay to all lower cross sections, particularly the $2s^2 2p^2\ ^1D$ which has a cross section at this energy significantly larger than $2s2p^3\ ^3D$, and $2s^2 2p^2\ ^1S$ which has a cross section almost as large as $2s2p^3\ ^3D$. This must be Auger decay and not simply interchannel coupling because the lower cross sections are larger than the $2s2p^3\ ^3D$. Thus, the cross section for the single-electron autodetachment process is much smaller than for the two-electron Auger processes.

The ^2P partial cross section, Fig. 2, shows a slow but significant rise from threshold, essentially all from the p wave. The striking difference between the ^2P and ^2D cross sections is due to the rather different locations of the $2s2p^4\ ^2P$ and ^2D states. Rough calculations show that the $2s2p^4\ ^2P$ state lies at much higher energy than the ^2D, but is also an order of magnitude stronger. The $2s2p^4\ ^2D$ state lies near to the channel threshold, but the $2s2p^4\ ^2P$ almost 6 eV higher. Further, owing to the characteristics of negative ions as compared to neutral atoms, i.e., the nl designations of states are much more approximate, the $(2s2p^3\ ^3D)3p\ ^2P$ state lies *below* the $2s2p^4\ ^2P$ state by about 4 eV, and it is significantly stronger (but still a factor of 4 weaker than $2s2p^4\ ^2D$), so this must be the more important contributor to the ^2P shape resonance. In essence, only the leading edge is seen in the energy range investigated here.

The ^2F channel, Fig. 4, shows a near-threshold p-wave maximum which cannot be associated with $2s2p^4$ since $2s2p^4$ has no ^2F multiplet. Thus, the significant near-threshold maximum in this cross section is probably due to a $2s \rightarrow 3p$ transition, i.e., a $2s2p^3 3p\ ^2F$ resonance. The primary mode of decay of this resonance is single-electron autodetachment to the $2s2p^3\ ^3D$ state of neutral carbon. No Auger transitions to either of the $2s^2 2p3s$ states within the ^2F partial cross section manifold are seen; this is because such an Auger process requires a very improbable three-particle transition. Auger transitions to $2s^2 2p^2\ ^1D$ and $2s^2 2p^2\ ^3P$ are seen in Fig. 4, but they are not very significant since the $2s^2 2p^2\ ^1D$ and $2s^2 2p^2\ ^3P$ partial cross sections in the ^2F channel are quite significant in this energy range.

7. Between the $2s2p^2 3s\ ^1P$ and the $2s2p^3\ ^3P$ thresholds

In this energy region there are six new states of neutral carbon that become energetically accessible in the photodetachment process, as shown in Figs. 1–4. The cross sections for populating each of these states are quite small in this energy region, no more than a few tenths of a megabarn. This is because none of the transitions to the various newly accessible final states, $2s2p^2 3s\ ^1P$, $2s^2 2p3p\ ^3D$, ^3S, ^3P, ^1D, and ^1S can proceed via a single-particle transition. Thus, photodetachment to these states of carbon is only possible through the influence of electron-electron correlation. Since these cross sections are so small, they have no appreciable effects on the lower cross sections.

8. Above the $2s2p^3\ ^3P$ threshold

The newly open channel in this region, populating the $2s2p^3\ ^3P$ state of neutral carbon, shows a significant near-threshold shape resonance. This resonance arises from the ^2P and ^2D partial cross sections, as seen in Figs. 2 and 3, respectively; the ^2F partial cross section, seen in Fig. 4, is extremely small. To understand this behavior, note that this state cannot be reached directly via a one-electron transition, as indicated in Table II; ejection of a $2s$ electron plus excitation of the $2p^3$ complex from ^2D, as it is in the initial state, to ^2P, as it must be in the final $2s2p^3$ state of carbon to couple to ^3P, is required. Then, since there are no other very strong channels in this energy region to induce significant mixing in these cross sections via interchannel coupling, the direct photodetachment cross sections to the continuum are small. Thus, the large ^2P and ^2D partial cross sections must be due to above-threshold (shape) resonances. Furthermore, the only *single-electron* excitations that can lead to the $2s2p^3\ ^3P$ state of neutral carbon are to $2s2p^4\ ^2P$ and ^2D

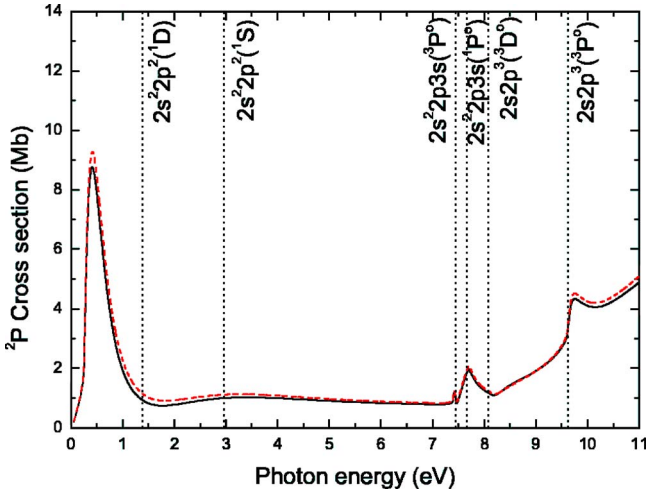

FIG. 5. (Color online) Total ^2P photodetachment cross sections of the excited ^2D state of C^- as a function of photon energy calculated in length (solid line) and velocity (dashed line) gauges. The vertical dotted lines represent the various thresholds.

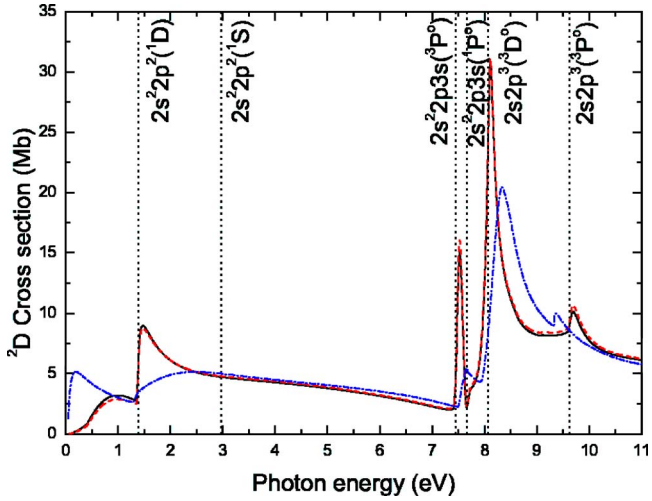

FIG. 6. (Color online) Total ^2D photodetachment cross sections of the excited ^2D state of C^- as a function of photon energy calculated in length (solid line) and velocity (dashed line) gauges. The vertical dotted lines represent the various thresholds. Also shown is an earlier theoretical result [11] (dot-dashed line).

states of the negative ion. It is evident, then, that the threshold resonances in the ^2P and ^2D partial cross sections have significant $2s2p^4$ character. This further supports the notion, discussed earlier, that the states of the negative ion are very mixed so that a number of different states have appreciable $2s2p^4$ character. Furthermore, since this $2s2p^4$ state has no ^2F multiplet, it is clear why the ^2F partial cross section does not exhibit this threshold feature.

These ^2P and ^2D resonances can decay not only to the $2s2p^3\ ^3P$ state of neutral carbon, but to almost all lower states as well; this Auger decay of a shape resonance is seen quite clearly in Figs. 2 and 3.

B. ^2P, ^2D, and ^2F cross sections

The partial photoionization cross sections, presented and discussed above, can also be summed over final states of neutral carbon to produce total ^2P, ^2D, and ^2F photodetachment cross sections. These are of interest because the sum is over the interacting channels (cross sections with different final-state angular momentum symmetries do not interact) which provides another view of how the interchannel coupling affects the results. In addition the total ^2D photodetachment cross section resulting from a previous calculation has been reported [11] and can be compared with the present result.

The calculated total ^2P photodetachment cross section is shown in Fig. 5. This cross section is dominated by the $2p \rightarrow 3s$ shape resonance near threshold, and some smaller shape resonances at higher energies, along with an increase starting at about 8 eV which is due to a very broad shape resonance with significant $2s2p^4$ character, as discussed above. Both length and velocity results are presented and they are seen to be in excellent agreement, thereby giving further support to the accuracy of the present results.

The total ^2D photodetachment cross section is presented in Fig. 6 where it is seen that this cross section has a rather different character from the ^2P. The threshold behavior is completely different, and the shape resonances at the higher energies are much stronger and sharper. In addition, there is no broad higher-energy resonance as in the ^2P case. Note also that over most of the energy range shown, the ^2D cross section is significantly larger than the ^2P; this is due principally to statistical factors which favor the ^2D final state of the carbon-plus-photoelectron system over the ^2P by a factor of 5/3. In the ^2D cross section too, excellent agreement is found between length and velocity calculations.

Also shown in Fig. 6 is the result of a previous calculation [11] which was presented only in the length formulation. Major differences are seen between the previous and present results, particularly in the threshold region. The resonance peak heights in the 7–10 eV region differ by factors of 2 or 3, and near threshold, the two results are not even qualitatively similar.

The total ^2F photodetachment cross section is given in Fig. 7 which shows that this cross section is dominated by a $2p \rightarrow 3d$ shape resonance in the threshold region, and a smaller $2s \rightarrow 3p$ shape resonance around 8.2 eV. The general background cross section is the largest of the three final symmetries owing partially to the statistical factor that favors ^2F over ^2D by a factor of 7/5. Here, too, agreement between length and velocity results is seen to be quite good.

C. Total photodetachment cross section

The total photodetachment cross section for the excited ^2D state is presented in Fig. 8. Since this cross section is the sum of those given in Figs. 5–7, the origin of all of the features is clear. In addition, since the individual contributions to this cross section all exhibited excellent agreement between length and velocity cross sections, this agreement is found in the total cross section as well, as is seen.

The result of the earlier calculation [11] is also shown in Fig. 8. From the comparison it is seen that the two results

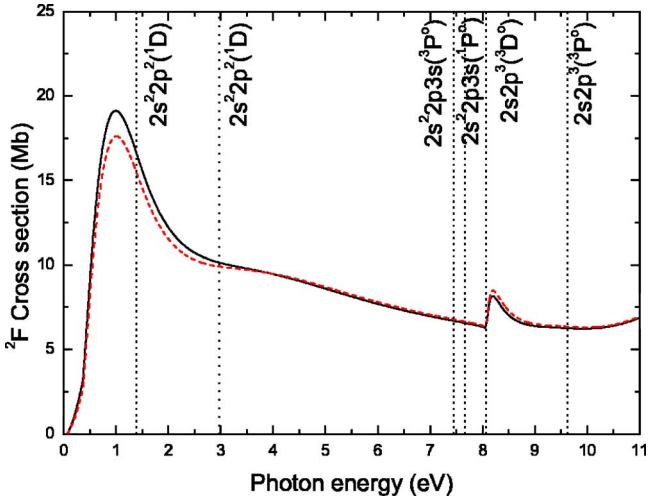

FIG. 7. (Color online) Total ^2F photodetachment cross sections of the excited ^2D state of C^- as a function of photon energy calculated in length (solid line) and velocity (dashed line) gauges. The vertical dotted lines represent the various thresholds.

agree qualitatively above a photon energy of about 3 eV, but with significant quantitative differences. Below this energy, the two results are completely different, both quantitatively *and* qualitatively. The differences between the present results and the earlier calculation are believed to be due to several factors: possible convergence difficulties in the earlier version of the *R*-matrix code, particularly at low energy; and the basis set in the earlier calculation, used to expand the wave functions of the initial state of C^- and the states of neutral carbon, was too small to adequately represent these wave functions. These difficulties were also present in the earlier calculation of the photodetachment of the *ground* state of C^-, as shown earlier [10]. Consequently, it is expected that our present results are the more accurate.

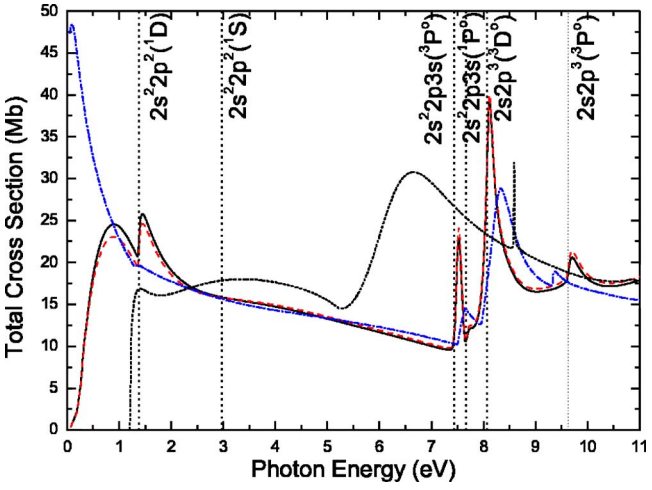

FIG. 8. (Color online) Total photodetachment cross sections of the excited ^2D state of C^- as a function of photon energy calculated in length (solid curve) and velocity (dashed curve) gauge, along with the ground ^4S cross section (dotted curve) [10] for comparison. Also shown is the earlier theoretical ^2D result [11] (dot-dashed curve). The vertical line represent the various detachment thresholds to the states of neutral C.

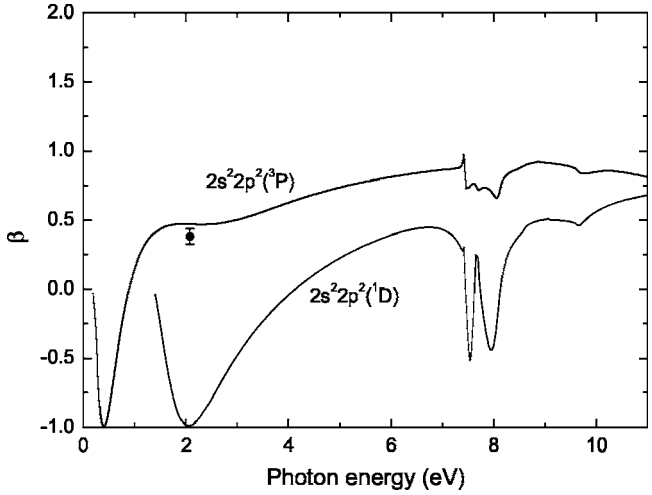

FIG. 9. Photoelectron angular distribution asymmetry parameter β calculated for photodetachment to $2s^22p^2\ ^2P$ and $2s^22p^2\ ^1D$ states of C. Since length and velocity results are so similar, only length is shown. Also shown is the experimental point measured for the $2s^22p^2\ ^3P$ state at 2.076 eV [16].

Also shown in Fig. 8 is the total photodetachment cross section for the ground state of C^- [10]. The magnitude is seen to be similar to the present case, indicating that the overall oscillator strength in this energy region is about the same for both the ground and excited states, but the details of the distribution differ markedly for both (angular momentum) geometric reasons, *and* dynamical reasons.

D. Photoelectron angular distributions

The photoelectron angular distribution for photodetachment to state j of neutral C is given, for linearly polarized incident light, by [26]

$$\frac{d\sigma_j}{d\Omega} = \frac{\sigma_j}{4\pi}[1 + \beta_j P_2(\cos\theta)], \tag{8}$$

where σ_j is the integrated cross section for producing state j, $P_2(x)=(3x^2-1)/2$, and β_j is the asymmetry parameter; clearly, from Eq. (8), the angular distribution is determined by β_j which can vary between -1 and 2. The calculation of the β_j for each case was performed using the angular momentum transfer formalism [26]. Using this analysis, it was found that for three of the channels, $2s^22p^2\ ^1S$, $2s^22p3p\ ^3S$, and $2s^22p3p\ ^1S$, $\beta_j=-1$, independent of energy; these are known as parity-unfavored transitions. The rest of the β_j's vary with energy owing to the interference among the various partial waves leading to each of the states of C.

The results of our calculation for photodetachment to the ground $2s^22p^2\ ^2P$ state of C is shown in Fig. 9. Near threshold, the (isotropic) *s* wave dominates, so the angular distribution is isotropic which means $\beta=0$, as seen; this threshold value is a characteristic of *all* photodetachment channels in which an *s* wave is allowed. Above threshold, the behavior of β is dictated mostly by the Cooper-Zare-like interference between the *s* and *d* waves, and to some extent by the interference among the various *d* waves; the *g* wave in the ^2F

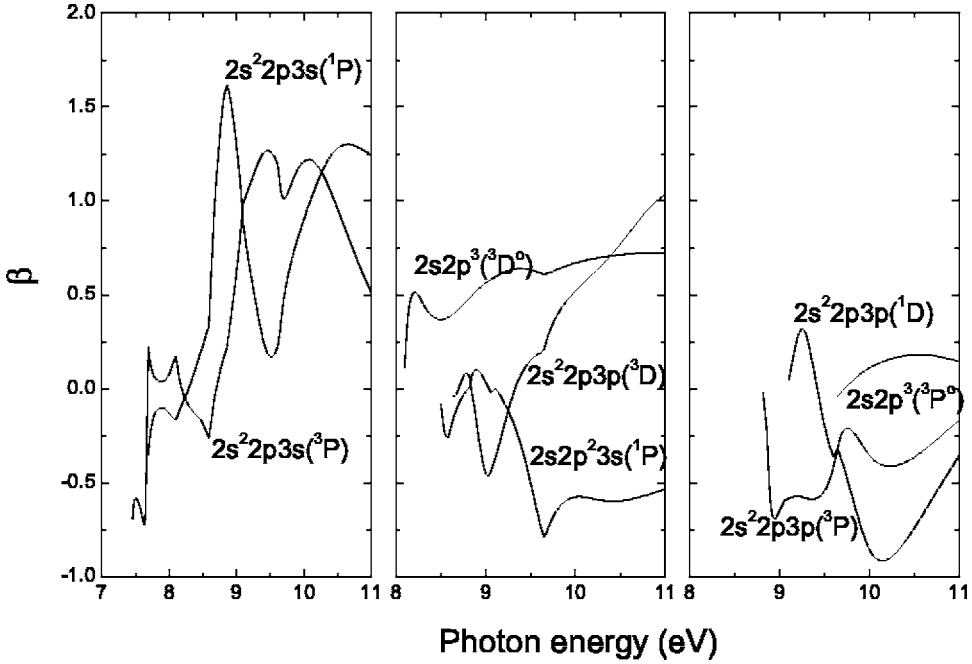

FIG. 10. Photoelectron angular distribution asymmetry parameter β calculated for photodetachment to $2s^22p3s\ ^3P$ and ^1P states of C (left panel), $2s2p^3\ ^3D$, $2s2p^23s\ ^1P$, and $2s^22p3p\ ^3D$ (center panel), and $2s^22p3p\ ^3P$, ^1D and $2s2p^3\ ^3P^o$ (right panel). Since length and velocity results are so similar, only length is shown.

channel plays almost no part. With increasing energy, the *s-d* interference terms in the expression for β, which enter with a negative sign, cause the value to decrease as seen; owing to the nature of negative ions, the cosine of the phase shift difference in this threshold region is near unity. With further increase in energy, the *d* waves start to dominate and β tends toward the value of unity, characteristic of a $p \rightarrow d$ transition [27]. However, the various interchannel couplings and resonances, as discussed above in connection with the subshell partial cross sections, along with the fact that the $p \rightarrow s$ does not entirely vanish, means that the approach to unity is only approximate, but, as seen, qualitatively valid.

Also shown is the experimental point measured at 2.076 eV [16]. It is clearly seen that agreement between theory and experiment is really quite good. Thus, although it is just a single energy, the agreement is is indicative of a quantitatively accurate theory.

A similar pattern emerges for the transition to the excited $2s^22p^2\ ^1D$ state of C, also shown in Fig. 9. Detailed differences in the matrix elements lead to the quantitative difference with the previous case at the lower energies. In the region around 8 eV, the significant structure of β is the result of the autoionization from the $2s^22p3s\ ^3P$ and $2s2s^4\ ^3P$, discussed above in connection with the partial cross sections.

The calculated β parameters for photodetachment to the $2s^22p3s$ states of C are shown in Fig. 10 where a completely different pattern emerges. In these cases, the dominant transitions in the threshold region involve *p* waves. Then, since the transitions involving the *p* waves contribute to more than one value of the angular momentum transfer [26], the threshold values are not fixed; depending upon the details of the *p*-wave matrix elements to the various possible channels, as listed in Table II, the angular momentum transfer analysis shows that the threshold value lies between 0.2 (the value for the parity-favored transition) and −1 (for the parity-unfavored transition). As seen in Fig. 10, this is indeed the case. In addition, these channels can only occur through the action of correlation, i.e., as seen in Table II, no single-particle transition is possible. Thus the matrix elements are small and easily perturbed by the interchannel coupling of other channels, leading to the strong dependence of these β parameters on energy, as seen.

The β parameter for photodetachment to $2s2p^3\ ^3D$ also shown in Fig. 10 is of particular interest because this channel is dominated by single-particle $s \rightarrow p$ in each of the final-state manifolds ^2P, ^2D, and ^2F. A single $s \rightarrow p$ transition is known to result in $\beta=2$, independent of energy; and if the dipole matrix elements to each of the final-state manifolds were the same, this would still be true [26]. Looking at Fig. 10, however, it is clear that nowhere in the energy range considered is β for this channel even close to the value 2. Thus, β gives a clear signature that there are profound dynamical differences among the three possible $s \rightarrow p$ matrix elements. The dynamical differences are seen in the cross sections for photodetachment to the $2s2p^3\ ^3D$ state, shown in Figs. 2–4, where the ^2P partial cross section differs dramatically both qualitatatively and quantitatively from the ^2D and ^2F. Furthermore, since β is so far from the value 2, it is evident that these dynamical differences continue to much higher energies. A similar situation, strong deviation of β from the value of 2 for photoabsorption by an *s* electron, was predicted some time ago for 3*s* photoionization from the neutral Cl atom [28], and this prediction has been recently verified [29]. From the point of view of the angular momentum transfer analysis, there are three possible values of the angular momentum transfer, j_t, and the associated β parameters take on the values 2, −1, and 0.2; the β parameter for the channel is a linear combination of these values weighted by the cross section for the particular value of j_t [26]. It would be most instructive to look at the β parameter for this channel experimentally.

The next four channels shown in Fig. 10, photodetachment to the $2s2p^23s\ ^1P$, $2s^22p3p\ ^3D$, ^3P, and ^1D, all represent detachment plus excitation and, as seen above, exhibit

relatively small cross sections. In each case there is a transition to an s wave in the final state; thus, by the arguments given above, the β parameter for each of these transitions must be zero at threshold. This is borne out in Fig. 10. Further, in each case, with increasing energy the final-state d wave becomes important (or even dominant), resulting in the strongly energy-dependent β parameters seen owing to the interferences among these alternate channels. The cases are further complicated by the interchannel coupling which affects particularly channels with small cross sections [30,31].

β corresponding to photodetachment to the $2s2p^3\ ^3P$ state of C is also shown in Fig. 10. This differs markedly from the transition to the $2s2p^3\ ^3D$ state in that direct single-particle transitions are forbidden. Thus except for transitions through the $2s2p^4$ resonances, the dipole matrix elements are quite small. Furthermore, it has been found that although final state f waves are possible (cf. Table II), they are significantly smaller than the p waves; the latter dominate the cross section and the β parameter. Looking only at the p waves then, two values of j_t are possible corresponding to β's of -1 and 0.2. Thus, as predicted previously [26], the β parameter for this transition *must* lie between these two values. This is indeed seen in Fig. 10. Furthermore, unlike the transition to the $2s2p^3\ ^3D$ state, where the β parameter will approach the value of 2 at high enough energy, for this case β will *never* approach 2, but rather the value of 0.2 at high energy. This is another case that would be of great interest to study experimentally.

IV. CONCLUDING REMARKS

In this paper is presented an accurate and comprehensive study of outer-shell photodetachment of the excited ^2D state of C^-. The good agreement of *ab initio* energies with experiment, the agreement of the cross section and β parameter with experiment (at a single energy) and the excellent agreement between length and velocity results all attest to the accuracy. Interchannel coupling within each of the final-state manifolds ^2P, ^2D, and ^2F were found to be of crucial importance in the photodetachment process, and initial-state correlation was also seen to be of importance. The β parameters were seen to be most strongly affected by electron-electron correlation as well. In addition, a previous calculation [11] has been corrected. Numerous shape (above-threshold) resonances have been identified, and many more examples of Auger decay of shape resonances are exhibited. It would be most useful if experimental photodetachment studies over a range of energies were performed for this excited negative ion, looking at both total and partial cross sections, as well as photoelectron angular distributions, the latter particularly in cases of photodetachment of the inner $2s$ electron.

ACKNOWLEDGMENTS

Helpful discussions with Dave Pegg are acknowledged. The work of H.L.Z. was supported by NASA, NSF, and IDRIS. The work of S.T.M. was supported by DOE, Division of Chemical Sciences, Basic Energy Sciences.

[1] B. M. Smirnov, *Negative Ions* (McGraw-Hill, New York, 1982).
[2] S. J. Buchman and C. W. Clark, Rev. Mod. Phys. **66**, 539 (1994), and references therein.
[3] V. K. Ivanov, J. Phys. B **32**, R67 (1999).
[4] D. J. Pegg, Rep. Prog. Phys. **67**, 857 (2004).
[5] H. P. Saha and R. N. Compton, Phys. Rev. Lett. **64**, 1510 (1990).
[6] J. Xi and C. F. Fischer, Phys. Rev. A **53**, 3169 (1996).
[7] D. S. Kim, H. L. Zhou, and S. T. Manson, Phys. Rev. A **55**, 414 (1997).
[8] H. L. Zhou, S. T. Manson, L. V. Ky, A. Hibbert, and N. Feautrier, Phys. Rev. A **64**, 012714 (2001).
[9] R. C. Bilodeau, J. D. Bozek, A. Aguilar, G. D. Ackerman, G. Turri, and N. Berrah, Phys. Rev. Lett. **93**, 193001 (2004).
[10] H. L. Zhou, S. T. Manson, A. Hibbert, L. V. Ky, N. Feautrier, and J.-C. Chang, Phys. Rev. A **70**, 022713 (2004).
[11] C. A. Ramsbottom, K. L. Bell, and K. A. Berrington, J. Phys. B **26**, 4399 (1993).
[12] N. Miura, T. Noro, and F. Sasaki, J. Phys. B **30**, 5419 (1997).
[13] G. F. Gribakin, A. A. Gribakina, B. V. Gultsev, and V. K. Ivanov, J. Phys. B **25**, 1757 (1992).
[14] G. Yu. Kashenock and V. K. Ivanov, Phys. Lett. A **245**, 110 (1998).
[15] D. H. Lee, W. D. Brandon, D. J. Pegg, and D. Hanstorp, Phys. Rev. A **56**, 1346 (1997).
[16] D. J. Pegg, C. Y. Tang, J. Dellwo, and G. D. Alton, J. Phys. B **26**, L789 (1993).
[17] P. G. Burke and K. A. Berrington, *Atomic and Molecular Process: An R-matrix Approach* (Institute of Physics, Bristol, 1993).
[18] K. A. Berrington, W. Eissner, and P. N. Norrington, Comput. Phys. Commun. **92**, 290 (1995).
[19] A. Hibbert, Comput. Phys. Commun. **9**, 141 (1975).
[20] E. Clementi and C. Roetti, At. Data Nucl. Data Tables **14**, 177 (1974).
[21] L. V. Ky, P. Faucher, A. Hibbert, J.-M. Li, Y.-Z. Qu, J. Yan, J. C. Chang, and F. Bely-Dubau, Phys. Rev. A **57**, 1045 (1998).
[22] L. V. Ky, P. Faucher, H. L. Zhou, A. Hibbert, Y.-Z. Qu, J. M. Li, and F. Bely-Dubau, Phys. Rev. A **58**, 3688 (1998).
[23] H. L. Zhou, S. T. Manson, L. V. Ky, P. Faucher, F. Bely-Dubau, A. Hibbert, S. Diehl, D. Cubaynes, J.-M. Bizau, L. Journel, and F. W. Wuilleumier, Phys. Rev. A **59**, 462 (1999).
[24] M. Scheer, R. C. Bilodeau, C. A. Brodie, and H. K. Haugen, Phys. Rev. A **58**, 2844 (1998).
[25] F. Rohrlich, Astrophys. J. **129**, 441 (1959).
[26] S. T. Manson and A. F. Starace, Rev. Mod. Phys. **54**, 389 (1982).
[27] S. T. Manson, J. Electron Spectrosc. Relat. Phenom. **1**, 413 (1973).
[28] A. F. Starace, R. H. Rast, and S. T. Manson, Phys. Rev. Lett. **38**, 1522 (1977).
[29] S. B. Whitfield, K. Kehoe, M. O. Krause, and C. D. Caldwell, Phys. Rev. Lett. **84**, 4818 (2000).

[30] E. W. B. Dias, H. S. Chakraborty, P. C. Deshmukh, S. T. Manson, O. Hemmers, P. Glans, D. L. Hansen, H. Wang, S. B. Whitfield, D. W. Lindle, R. Wehlitz, J. C. Levin, I. A. Sellin, and R. C. C. Perera, Phys. Rev. Lett. **78**, 4553 (1997).

[31] D. L. Hansen, O. Hemmers, H. Wang, D. W. Lindle, P. Focke, I. A. Sellin, C. Heske, H. S. Chakraborty, P. C. Deshmukh, and S. T. Manson, Phys. Rev. A **60**, R2641 (1999).

[32] http://physics.nist.gov/cgi-bin/AtData/main_asd